# Observation of macroscopic valley-polarized monolayer exciton-polaritons at room temperature

N. Lundt[1], S. Stoll[1], P. Nagler[2], A. Nalitov[3], S. Klembt[1], S. Betzold[1], J. Goddard[1], E. Frieling[1], A.V. Kavokin[3,4], C. Schüller[2], T. Korn[2], S. Höfling[1,5] and C. Schneider[1]

[1]*Technische Physik and Wilhelm-Conrad-Röntgen-Research Center for Complex Material Systems, Universität Würzburg, D-97074 Würzburg, Am Hubland, Germany*

[2]*Department of Physics, University of Regensburg, Regensburg D-93040, Germany*

[3]*Physics and Astronomy School, University of Southampton, Highfield, Southampton, SO171BJ, UK*

[4]*SPIN-CNR, Viale del Politecnico 1, I-00133 Rome, Italy*

[5]*School of Physics and Astronomy, University of St. Andrews, St. Andrews KY 16 9SS, United Kingdom*

**In this letter, we address the chiral properties of valley exciton-polaritons in a monolayer of $WS_2$ in the regime of strong light-matter coupling with a Tamm-Plasmon resonance. We observe that the effect of valley polarization, which manifests in the circular polarization of the emitted photoluminescence as the sample is driven by a circularly polarized laser, is strongly enhanced in comparison to bare $WS_2$ monolayers, and can even be observed under strongly non-resonant excitation at ambient conditions. In order to explain this effect in more detail, we study the relaxation and decay dynamics of exciton-polaritons in our device, elaborate the role of the dark state and present a microscopic model to explain the wave-vector-dependent valley depolarization by electron-hole exchange interaction and the linear polarization splitting inherent to the microcavity. We believe that our finding are crucial for designing novel polariton-valleytronic devices which can be operated at room temperature.**

Excitons which are hosted in two-dimensional atomic crystals of transition metal dichalcogenides (TMDCs) have a variety of intriguing optical properties, which puts them in the focus of advanced light-matter coupling. This includes their enormous exciton binding energies up to 550 meV[1,2], their ultra-fast dipole transitions[3] as well as the materials' unique spin- and valley-related properties[4–7]. The latter are a direct consequence of the broken inversion symmetry of the monolayers in combination with a strong spin-orbit coupling inherited by the transition metal atoms, lifting the polarization degeneracy of the high-symmetry K points at the corners of the Brillouin zone. Thus, excitons at the K and K' point are tagged with a valley index, or valley pseudospin, which is more robust with respect to depolarization as the exciton pseudospin conventional III-V semiconductors. The coupling of spin and valley degree of freedom in TMDC monolayers, in principle, allows to build electronic and opto-electronic devices based with rich polarization- and spin features, giving rise to the field of valleytronics[7]. Recently, it has been shown that cavity effects can enhance the time-averaged degree of exciton and trion valley polarization[8–11], which is partly explained by a speed-up of the relaxation dynamics of excitons. However, no detailed time-resolved measurements have been presented along with this explanation. Moreover, the role of the dark exciton state, which is considered crucial for a high degree of valley polarization in tungsten-based TMDCs[12], has not been elaborated in detail. In addition to the electron-hole exchange interaction, the artificial magnetic field provided by the polarization splitting of the cavity resonances acts as depolarization mechanism which has to be taken into account. Here, we investigate the relaxation and valley depolarization of valley-tagged exciton-polaritons evolving in a Tamm-plasmon structure[13,14] with an integrated monolayer of $WS_2$ at ambient conditions. Time-resolved photoluminescence measurements were carried out to shed more light onto the relaxation dynamics of the observed exciton-polaritons. We discuss the role of the interplay between dark and bright state, which is affected by a dramatic change of the bright state dispersion relation in the polariton framework. Finally, we present a theoretical model of the depolarization mechanism along the dispersion relation, which explains the measured, distinct polarization dependence on the in-plane wave vector.

**Monolayer characterization**

The investigated $WS_2$ monolayer was mechanically exfoliated from a bulk crystal and subsequently transferred onto a distributed Bragg reflector (DBR) with a viscoelastic polymer stamp. The monolayer was identified by its optical contrast and its distinct photoluminescence (PL). The DBR is composed of 10 $SiO_2/TiO_2$ layers with thicknesses of 105 nm/65 nm, respectively. The photoluminescence of the monolayer (on top of the DBR), presented in Fig. 1a, was recorded under 568 nm excitation (continuous-wave laser (Coherent sapphire), 0.7 mW) and ambient condition. The spectrum shows a clear resonance at 618.57 nm/ 2.004 eV with a linewidth (FWHM) of 29 meV, which we attribute to the neutral excitonic transition of the A excitons. The low-energy shoulder of the peak can be assigned to a trionic transition with an exciton-trion energy splitting of 42 meV, which strongly grows in intensity at lower sample temperatures, in line with previous observations[15]. First, we study the polarization properties of our bare monolayer as a function of the detuning of the pump laser and temperature. Figure 1a depicts a polarization-resolved photoluminescence spectrum of the monolayer exciton recorded at 290 K. The sample was excited with a $\sigma^+$-polarized laser (568nm) and the luminescence is detected in $\sigma^+/\sigma^-$ configurations. The degree of circular polarization (DOCP) is calculated via $P = \frac{I(\sigma^+)-I(\sigma^-)}{I(\sigma^+)+I(\sigma^-)}$, where I is the integrated PL intensity. The degree of circular polarization of the emitted light as a function of

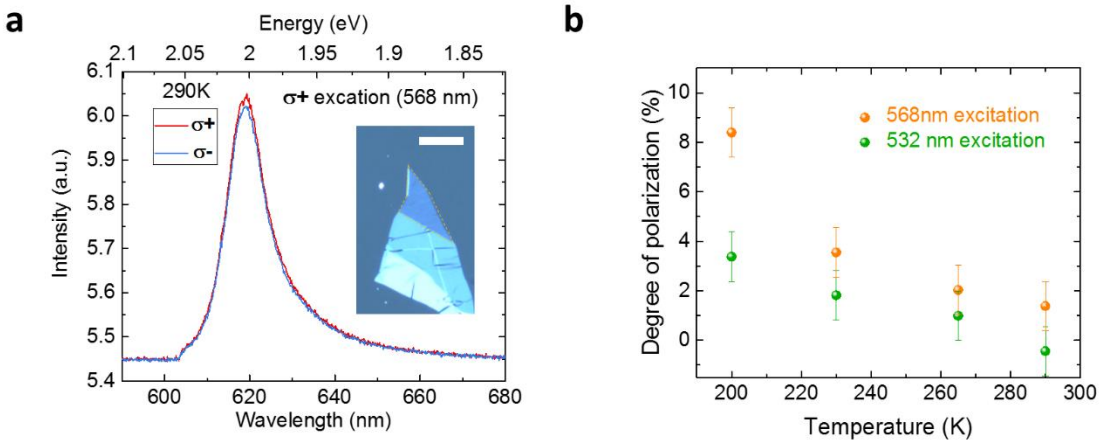


temperature and excitation energy (532 nm vs. 568nm excitation) is plotted in Fig 1b. While the increase in P with decreasing temperature and an excitation energy closer to the exciton resonance is in excellent

**Figure 1 | Characterization of $WS_2$ monolayer** a) PL spectra of a monolayer (shown and marked by yellow lines in the inset where the scale bar corresponds to 30 µm) at 290K under $\sigma^+$ polarized excitation at 568nm recorded in $\sigma^+/\sigma^-$ configurations. b) Degree of circular polarization as a function of temperature for 532 nm and 568 nm excitation wavelengths.

agreement with previous findings[16], we emphasize that no significant DOCP can be extracted at ambient conditions.

**Exciton-Polaritons**

The photonic Tamm structure is completed by capping the $WS_2$ monolayer by 70 nm of PMMA and evaporation of 40 nm of silver on top of the PMMA layer (Fig. 2a). A final $SiO_2$ layer was deposited to protect the silver layer from degradation. The bottom DBR supports a very high reflectivity of 99.97 % in a spectral range between 540 nm and 680 nm, and the photonic microstructure features a strong field enhancement close to the metallic interface (see Fig. 2b) at the monolayer location. This strong field enhancement makes such structures particularly interesting to study the physics of exciton-polaritons in solid state systems[17]. The layer thicknesses, illustrated in Fig. 2b as the sequence of the corresponding refractive indices, were designed to promote an optical mode energetically close to the exciton resonance and to spatially overlap with the monolayer. The resonance of the empty cavity was probed in a white light reflectivity measurement presented in Fig. 2c and corresponds to a quality factor of 120.

The formation of room-temperature exciton-polaritons in our device is confirmed by single-shot angle-resolved photoluminescence measurements in a back-Fourier plane imaging configuration (See supplementary S6). Utilizing a high magnification (50 x) microscope objective with a numerical aperture of 0.65 allows us to project an in-plane momentum range of up to 5.5 $\mu m^{-1}$ onto the CCD chip of our spectrometer in this imaging configuration[8]. For polarization measurements we use a λ/4 waveplate to generate $\sigma^+/\sigma^-$ polarized light and analyzed the emitted signal with a rotatable λ/4 waveplate followed by a linear polarizer. We used a non-polarizing beam splitter preserving s- and p-components by 98%. In addition, the incident laser was analyzed by a polarimeter at various positions in the optical path and the λ/4 waveplate was slightly corrected in order to compensate for the loss in degree of circular polarization at the beam splitter. This ensures a circular degree of polarization of more than 99.9%. The emitted light on the detection path is still subject to a relative error of 2%. The main error contribution is the laser power fluctuation on the order of 1%.

The luminescence which we collect from our device is depicted in Fig 2d). It features the typical, distinct dispersion relation of the lower branch of cavity exciton-polaritons, which emerge in the strong coupling

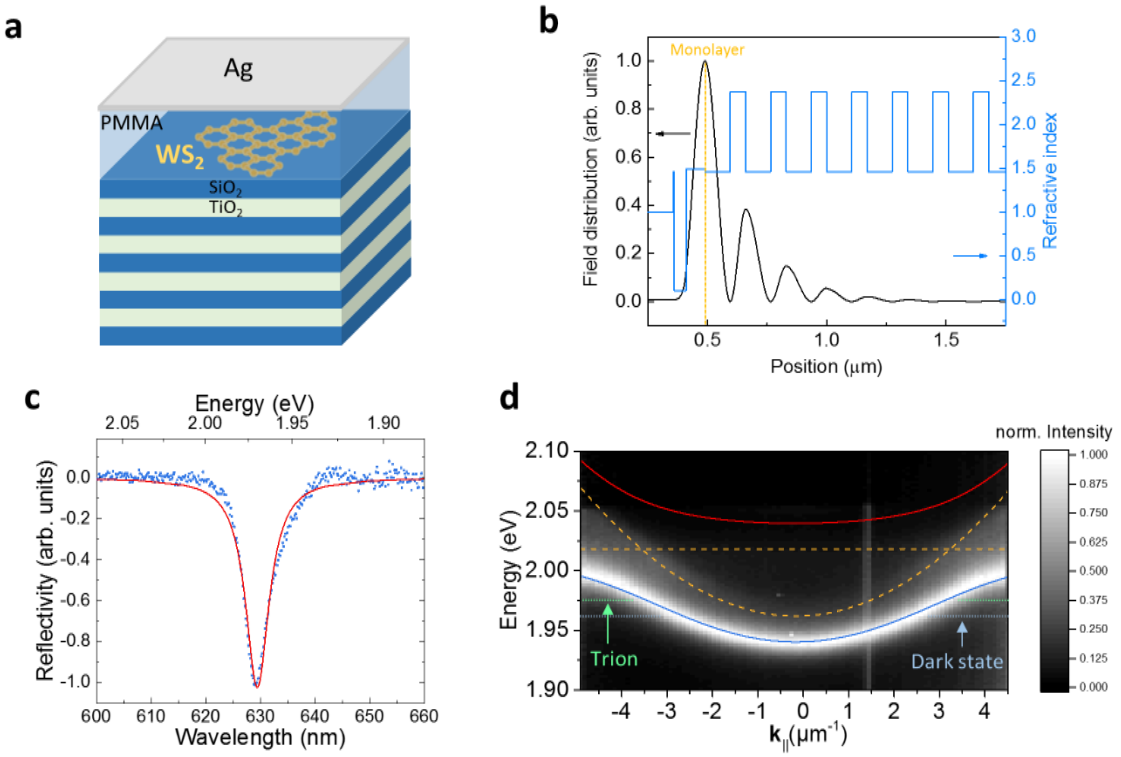


**Figure 2 | Exciton-Polaritons** a) Schematic illustration of the photonic structure with the integrated $WS_2$ monolayer. b) Layer sequence of the photonic structure illustrated by the corresponding refractive indices and the calculated optical field distribution within the photonic structure. The position of the monolayer in the photonic structure is marked as orange, dashed line. c) Measured reflectivity spectrum of the empty cavity at zero in-plane wave vector. The linewidth corresponds to a quality factor of 120. d) Exciton-polariton dispersion relation incl. a coupled oscillator fit. The upper and lower polariton branches are drawn in red and blue, respectively, where the uncoupled exciton and cavity modes are indicated by orange, dashed lines. Expected energies of trion and dark state are indicated in the background.

regime between excitons and cavity photons. At low k values, this dispersion is dominated by the low mass[18] of two-dimensional cavity photons (approx. $10^{-5}$ $m_e$, $m_e$ being the free electron mass), while its curvature features an inflection point at k~ 3.0 $\mu m^{-1}$. We can fit the dispersion with a two-coupled oscillator model[17], to extract the Rabi splitting and the exciton-photon detuning of our device. Here, we take advantage of the fact that we can observe the empty cavity dispersion as a faint photoluminescence branch in the background. This PL stems from edge regions of the monolayer and is weakly coupled to the cavity mode. The fit yields a Rabi splitting as large as 80 meV, and an exciton-photon detuning of -55 meV at k=0, which is in good agreement with previous findings on strongly coupled $WS_2$ monolayers in a micro-cavity considering a comparable mode volume[19]. The upper polariton branch cannot be observed due to its very low thermal population resulting from the large normal mode coupling strength.

We note that due to the large Rabi splitting, our polariton dispersion crosses both the (weakly coupled) trion resonance, as well as the dark exciton (55 meV below the exciton)[20]. Both resonances are indicated by arrows in Fig 2d). Neither the trion nor the dark state resonance are expected to carry enough oscillator strength at room temperature in order to strongly couple with the cavity mode. The small oscillator strength seems plausible since the resonances cannot be measured in absorption experiments at room temperature. Since the polariton bright state is now energetically favored and also carries significantly more oscillator strength, the PL intensity of the polariton branch governs the dispersion. However, since both resonances are in the perturbative regime with our cavity resonance, we believe that the weak coupling conditions can yield a transfer of populations to the polariton states.

**Exciton and Polariton Dynamics**

The fitting procedure also provides the light-matter coupling strength, which in turn can be used to assess the radiative lifetime of the $WS_2$ valley excitons. The Rabi splitting yields a direct connection with the exciton oscillator strength and the effective cavity length[21], which can be expressed as:

$$\Omega_R = 2 * \sqrt{\frac{2\Gamma_0 c}{n_c(L_{DBR} + L_C)}}$$

Here, $\Gamma_0$ represents the radiative decay of the excitons, $n_c$ is the effective index of the cavity and $L_{DBR} + L_C$ is the effective cavity length. c is the speed of light in free space. Introducing our system parameters (see supplementary information S1), we determine a radiative decay time as short as 220 fs. We note that this decay time is in good agreement with previous experimental studies on $WSe_2$ monolayers[3] and theoretical predictions[22]. In our case, we emphasize that our method allows us to solely probe the radiative decay time, as the non-radiative decay channels would not contribute to the light-matter coupling strength. In fact, a calculation of the lower polariton radiative lifetimes in our strongly coupled system yields values that are 3 - 9 times shorter as explained in supplementary S2.

In order to assess the full relaxation dynamics of our system, we perform streak-camera measurements on the bare $WS_2$ monolayer, as well as on the fully built cavity in the strong coupling regime. For this, the sample was excited by a frequency-doubled pulsed fiber laser system (TOPTICA TVIS, pulse length (FWHM) 180 fs, pulse repetition rate 80 MHz) tuned to a central wavelength of 568 nm, coupled into a 100x microscope objective and focused to a spot diameter of less than 1 µm on the sample surface. The PL from the sample was collected using the same objective and coupled into a grating spectrometer, where it was detected using a streak camera coupled to the spectrometer and electronically synchronized with the pulsed laser system. The temporal resolution of this setup (HWHM of the pulsed laser trace) is below 4 ps (see supplementary S6 for a schematic depiction of the setup).

Fig 3a depicts the photoluminescence decay curves of polariton states at high in-plane k-vectors (~ 5 $\mu m^{-1}$), often referred to as the reservoir, and of the polariton ground state (k=0 $\mu m^{-1}$). Both time traces exhibit two dominant exponential decay channels and a very weak third decay. The reservoir decay time constants $\tau_1$ and $\tau_2$ of 8.8 ps and 30.3 ps, respectively, are in excellent agreement with the reference measurement on the bare $WS_2$ monolayer (8.2 ps and 31.6 ps, respectively, see supplementary information S3). This is well in line with the highly excitonic character of the polaritons at high k-vectors and previous findings[23,24]. This also supports the idea that the scattering outside the light cone and close to light cone edge are not significantly affected. In contrast, the characteristic time constants decrease to 6.8 ps and 23.2 ps, respectively, in the polariton ground state. The third decay channel only makes up a minor fraction of the PL intensity (<1%) and is on the order of 100 ps in all measurements.

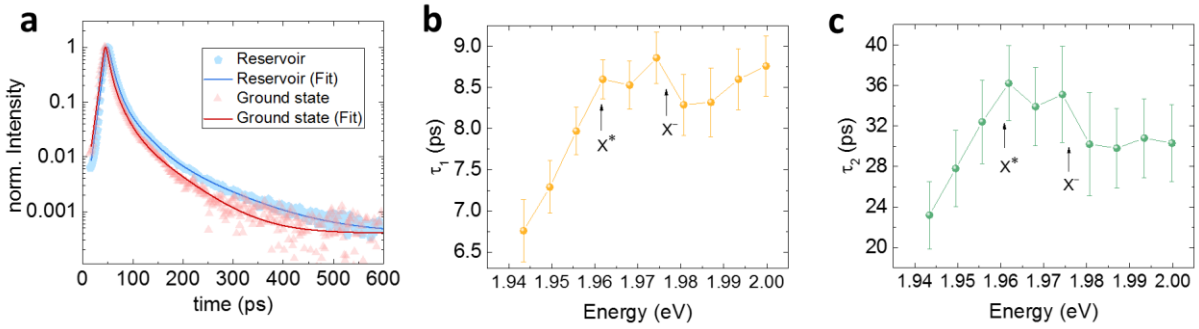


**Figure 3 | Relaxation dynamics** a) Decay curves of the polariton reservoir *(~ 5 $\mu m^{-1}$)* and the polariton ground state *( 0 $\mu m^{-1}$)* b) Time constant $\tau_1$ as a function of emission energy. c) Time constant $\tau_2$ as a function of emission energy. Expected energies of the dark state X* and trion $X^-$ are indicated.

In more detail, Figure 3b and 3c illustrate the decay constants $\tau_1$ and $\tau_2$ as a function of energy which is related to the in-plane wave vector through the dispersion relation. Here, the low-energy end at 1.94 eV represents the polariton ground state, whereas the high-energy tail at 2.01 eV is attributed to emission from the highly excitonic reservoir.

Interestingly, both time constants feature a decrease towards lower energies, as well as a slight increase between 1.96 eV and 1.975 eV. In fact, this increase occurs at energies where the polariton dispersion crosses the dark state and the trion resonances, which feature slower decay dynamics[25]. This indicates an indirect pumping mechanism from these weakly coupled states into the polariton states.

Because of the very fast radiative decay of the exciton and polariton states inside the light cone, we attribute the decay times as the depopulation dynamics of the original states from which excitons/polaritons scatter into the measured state. These states presumably lie outside the light cone or can be attributed to trion or dark states. Here, we attribute the first channel to fast, phonon-assisted carrier relaxation from outside of the light cone (followed by fast radiative decay) whereas the second, slower decay could be an indication for a transfer from the dark exciton state.

**Polariton Valley Polarization**

In the following, we address the spin- and valley-related properties of our polariton system via polarization-resolved spectroscopy. Here, we inject reservoir excitons non-resonantly via circularly polarized pump lasers with wavelengths of 532 nm or 568 nm, respectively, and measure the DOCP as a function of the polariton wave-vector. The results of this experiment, shown in Fig. 4a (532 nm excitation) and Fig 4b (568 nm excitation), are strikingly different to the case of the bare monolayer, where the DOCP is marginal at room temperature. For the case of 568 nm excitation wavelength, we observe a DOCP as large as 10 % from the polariton ground state at ambient conditions, which is slightly lower for the higher excitation energy (532 nm laser). These finding are well in line with very recent results[11]. We furthermore observe a distinct dependency of the DOCP on the in-plane wave vector. The

observation of this high circular polarization from the polariton states is, at first sight, surprising, since the system follows the dynamics of the bright exciton reservoir, which manifest in the comparable scattering dynamics for the bare monolayer and the polariton at high wave vectors and which we consider as strongly depolarized at 300 K (see Fig 1).

While the relaxation into the bright exciton/exciton-polariton states is almost completely depolarizing, the dark exciton state is considered to maintain the excitation polarization[12,26] as illustrated in Fig. 4c. While at zero in-plane wave vector the dark exciton has no oscillator strength, it significantly

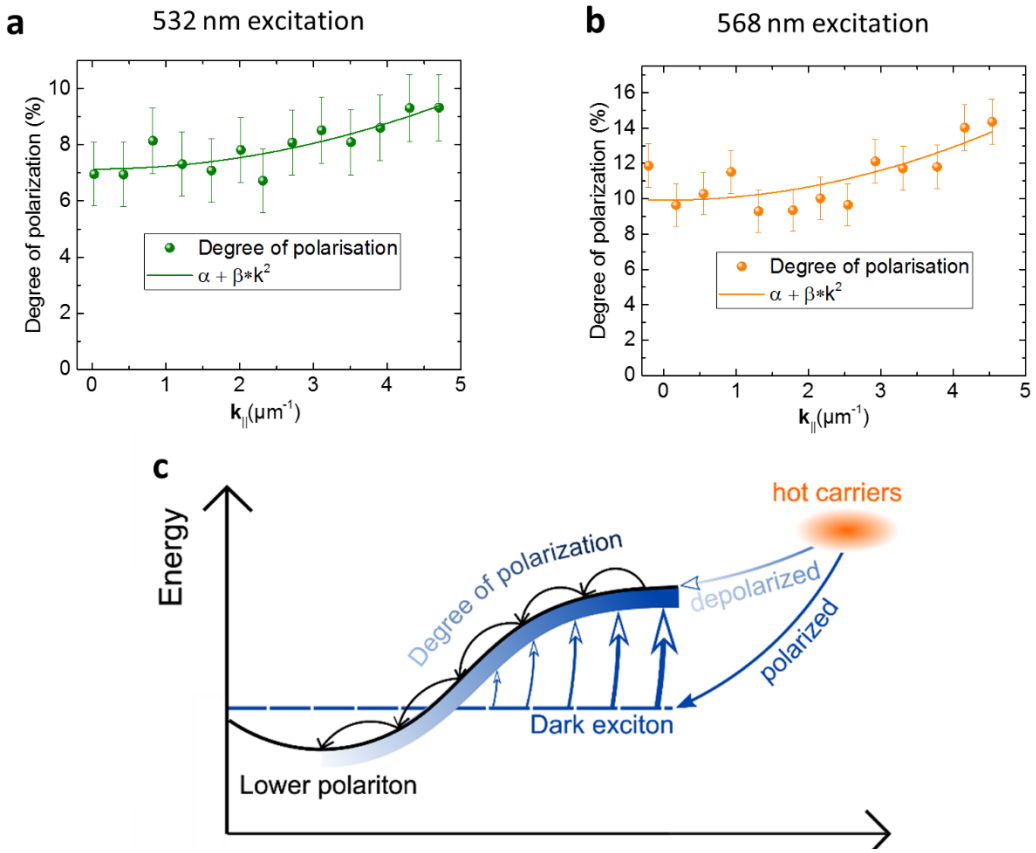


**Figure 4 | Polariton valley-polarization** a) Degree of circular polarization as a function of in-plane wave vector under 532 nm excitation. b) Degree of circular polarization as a function of in-plane wave vector under 568 nm excitation. c) Schematic model for polariton valley polarization.

accumulates oscillator strength at large in-plane momenta[27]. Hence, it is reasonable to assume that it can weakly couple to corresponding high-k polariton states (illustrated in Fig. 4c), followed by a radiative decay or a redistribution along the polariton branch. The coupling to the bright state is strongly enhanced

by the cavity effect, since emitted light from the dark state can be reabsorbed by the bright polariton state. In fact, the emission of the dark state should be enhanced when weakly coupled to the cavity mode, whereas the absorption by the bright polariton state is more likely since it should carry significantly more oscillator strength even at high wave vectors. Thus, we determine a second reservoir at large $k_{\parallel}$, which is robust against valley depolarization since dark excitons are not subject to strong exchange interactions[12]. (See supplementary information S4 for further details on the transfer from dark to bright state).

The transfer from the dark state can be followed by a redistribution of polaritons along the polariton branch. However, in this case the polarized polaritons are again subject to the strong exchange interactions, which can lead to valley depolarization during their redistribution. In the following, we provide a description and an analytic expression of the valley depolarization in our polariton system. Here, we consider a gas of free polaritons with parabolic dispersion. We will account for (1) acoustic phonon-assisted energy relaxation, which is dominant below the condensation threshold, and (2) Maialle-Silva-Sham-type spin relaxation stemming from the interplay of momentum-dependent effective magnetic field acting on the polariton pseudospin and stochastic elastic momentum scattering. The dynamics of spin relaxation in a polariton gas has been modelled numerically by solving the full set of Boltzmann kinetic equations[28]. In contrast, here we opted for a simplified analytical model with a very limited number of free parameters. We are interested in the analytical expression for the circular polarization of the polariton emission as a function of the in-plane momentum, for the stationary state corresponding to the CW pumping regime.

We discretize the continuous problem and reformulate it in terms of a ladder of discrete quantum states, where direct transitions are only allowed between the neighboring energy levels. We consider phonon assisted inelastic transitions for a polariton with the momentum **p** and neglected nonlinear effects caused by exciton-exciton scattering. In contrast to quantum-well-based microcavities, where the main contribution to phonon-assisted exciton energy relaxation stems from the phonons with momenta oriented along the growth direction[29], the TMDC atomic layers are only coupled to the substrate by the Van der Waals force, so that the excitons only emit in-plane phonons[30]. The characteristic energy lost in a single act of scattering that is taken as an interlevel distance in our model, is then derived from the

energy and momentum conservation rules. The rates of polariton transitions between the levels $\alpha_i = \alpha\, p_i^3$ depend on the wave vector via the exciton-phonon matrix element, the exciton Hopfield coefficient, and the density of polariton states.

The spin relaxation rate $\gamma_i$ is governed by the Maialle-Silva-Sham mechanism $\gamma_i = \Omega_i^2\, \tau$, where $\Omega_i$ is the value of the effective magnetic field and $\tau$ is the polariton transport time, which we assume as constant. The effective field $\Omega_i$ originates from the TE-TM splitting of the photonic polariton component and the long-range part of the electron-hole exchange acting on the excitonic component. In the vicinity of the polariton dispersion minimum the photonic component is dominant, hence, the effective field is given by the TE-TM splitting, which is quadratic in polariton momentum, allowing us to assume $\gamma_i = \beta\, p_i^4$.

This yields an analytical expression for the DOCP as a function of the momentum which reads

$$P(p) = P(0) + \frac{\beta}{2\alpha} p^2$$

As shown in Fig. 4a and 4b, our data can be well fitted by this expression, which confirms our initial assumptions about the important effect of both the electron-hole exchange interaction and the TE-TM splitting in our cavity on the spin-depolarization of valley excitons in TMDC based cavities.

Although our model succeeds to fit the experimental data very well, we note that direct polariton-polariton scattering from reservoir states must be taken into consideration in particular for large pump powers, where the exciton-exciton scattering and the bosonic stimulation become important. This process would result in a speed up in the relaxation dynamics, which is in fact observed for the ground state.

## Conclusion

In conclusion, our study sheds light onto the interplay between relaxation, depolarization and decay of valley exciton-polaritons. First, we demonstrate the formation of exciton-polaritons in a photonic microstructure with excitons in a $WS_2$ monolayer with a light-matter coupling strength of 80 meV,

corresponding with a purely radiative decay time of excitons as short as 220 fs. We find that the polariton scattering dynamics at high wave vector and close to the light cone edge are not strongly affected as compared to the bare monolayer, yet relaxation of polaritons towards the ground state is slightly enhanced even at modest densities. Despite the slow relaxation, we map out a significant enhancement of polaritonic valley polarization up to 14 % at high wave vectors. We attribute this increase to the cavity-enhanced transfer from dark exciton states to the polariton branch, which is more effective at high wave vectors. The polarization relaxation is explained within a microscopic model, which accounts for energy and spin-relaxation of exciton-polaritons in the presence of the linear polarization splitting of the micro cavity. We believe that our findings represent a major step towards harnessing spin-valley coupling in light-matter-coupled devices operated at room temperature.

This work has been supported by the State of Bavaria and the ERC (unlimit-2D), as well as the DFG via SFB689, GRK 1570 and KO3612/1-1. We thank S. Tongay for supporting this project. Correspondence and requests for materials should be addressed to Christian Schneider and Nils Lundt (christian.schneider@physik.uni-wuerzburg.de, nils.lundt@physik.uni-wuerzburg.de)

**References**


1. Ugeda, M. M. *et al.* Giant bandgap renormalization and excitonic effects in a monolayer transition metal dichalcogenide semiconductor. *Nat. Mater.* **13,** 1091–1095 (2014).

2. Chernikov, A. *et al.* Exciton Binding Energy and Nonhydrogenic Rydberg Series in Monolayer $WS_2$. *Phys. Rev. Lett.* **113,** 76802 (2014).

3. Poellmann, C. *et al.* Resonant internal quantum transitions and femtosecond radiative decay of excitons in monolayer $WSe_2$. *Nat. Mater.* **14,** 1–6 (2015).

4. Xiao, D., Liu, G.-B., Feng, W., Xu, X. & Yao, W. Coupled Spin and Valley Physics in Monolayers of $MoS_2$ and Other Group-VI Dichalcogenides. *Phys. Rev. Lett.* **108,** 196802 (2012).

5. Wang, Q. H., Kalantar-Zadeh, K., Kis, A., Coleman, J. N. & Strano, M. S. Electronics and optoelectronics of two-dimensional transition metal dichalcogenides. *Nat. Nanotechnol.* **7,** 699–712 (2012).

6. Cao, L. Two-dimensional transition-metal dichalcogenide materials: Toward an age of atomic-scale photonics. *MRS Bull.* **40,** 592–599 (2015).

7. Mak, K. F., Shan, J. Photonics and optoelectronics of 2D semiconductor transition metal dichalcogenides. *Nat. Photonics* **10,** 216–226 (2016).

8. Lundt, N. *et al.* Valley polarized relaxation and upconversion luminescence from Tamm-Plasmon Trion-Polaritons with a $MoSe_2$ monolayer. *2D Mater.* **4,** 25096 (2017).

9. Chen, Y., Cain, J. D., Stanev, T. K., Dravid, V. P. & Nathaniel, P. Valley-Polarized Microcavity Exciton-Polaritons in a Monolayer Semiconductor. *Nat. Photonics* **11,** 431–435 (2017).

10. Dufferwiel, S. *et al.* Valley-addressable polaritons in atomically thin semiconductors. *Nat. Photonics* 1–6 (2017). doi:10.1038/nphoton.2017.125

11. Sun, Z. *et al.* Optical control of room-temperature valley polaritons. *Nat. Photonics* (2017). doi:10.1038/nphoton.2017.121

12. Baranowski, M., Surrente, A., Maude, D. K., Ballottin, M., Mitioglu, A. A., Christianen, P. C. M., Kung, Y. C., Dumcenco, D., Kis, A., Plochocka, P. Dark excitons and the elusive valley polarization in transition metal dichalcogenides. *2D Mater.* **4,** (2017).

13. Lundt, N. *et al.* Room temperature Tamm-Plasmon Exciton-Polaritons with a $WSe_2$ monolayer. *Nat. Commun.* 1–6 (2016).

14. Hu, T. *et al.* Strong coupling between Tamm plasmon polariton and two dimensional semiconductor excitons. *Appl. Phys. Lett.* **110,** 51101 (2017).

15. Plechinger, G. *et al.* Identification of excitons , trions and biexcitons in single-layer WS2. *Phys. Status Solidi Rapid Res. Lett.* **461,** 457–461 (2015).

16. Hanbicki, A. T. *et al.* Anomalous temperature-dependent spin-valley polarization in monolayer $WS_2$. *Sci. Rep.* **6,** 18885 (2016).

17. Deng, H., Haug, H. & Yamamoto, Y. Exciton-polariton Bose-Einstein condensation. *Rev. Mod.*

*Phys.* **82,** 1489–1537 (2010).

18. Richard, M. The not-so-effective mass of photons in a planar optical cavity. *arXiv:1512.01130* 1–5 (2015).

19. Flatten, L. C. *et al.* Room-temperature exciton-polaritons with two-dimensional $WS_2$. *Sci. Rep.* 1–7 (2016).

20. Wang, G. *et al.* In-Plane Propagation of Light in Transition Metal Dichalcogenide Monolayers : Optical Selection Rules. *Phys. Rev. Lett.* **47401,** 1–7 (2017).

21. Savona, V., Andreani, L. C., Schwendimann, P. & Quattropani, A. Quantum well excitons in semiconductor microcavities: Unified treatment of weak and strong coupling regimes. *Solid State Commun.* **93,** 733–739 (1995).

22. Palummo, M., Bernardi, M. & Grossman, J. C. Exciton radiative lifetimes in two-dimensional transition metal dichalcogenides. *Nano Lett.* **15,** 2794–2800 (2015).

23. Perrin, M. *et al.* Relaxation dynamics of microcavity polaritons in the presence of an electron gas. *Phys. Status Solidi C Conf.* **2,** 3920–3923 (2005).

24. Senellart, P., Bloch, J., Sermage, B. & Marzin, J. Y. Microcavity polariton depopulation as evidence for stimulated scattering. *Phys. Rev. B - Condens. Matter Mater. Phys.* **62,** 263–266 (2000).

25. Wang, G. *et al.* Valley dynamics probed through charged and neutral exciton emission in monolayer WSe2. *Phys. Rev. B* **75413,** 1–6 (2014).

26. Plechinger, G. *et al.* Trion fine structure and coupled spin–valley dynamics in monolayer tungsten disulfide. *Nat. Commun.* **7,** 12715 (2016).

27. Wang, G. *et al.* In-plane Propagation of Light in Transition Metal Dichalcogenide Monolayers: Optical Selection Rules. *arxiv:1704.0534* (2017). at <http://arxiv.org/abs/1704.05341>

28. Kavokin, K. V., Shelykh, I. A., Kavokin, A. V., Malpuech, G. & Bigenwald, P. Quantum Theory of Spin Dynamics of Exciton-Polaritons in Microcavities. *Phys. Rev. Lett.* **92,** 17401 (2004).

29. Piermarocchi, C., Tassone, F., Savona, V., Quattropani, A. & Schwendimann, P. Nonequilibrium dynamics of free quantum-well excitons in time-resolved photoluminescence. *Phys. Rev. B* **53,** 15834–15841 (1996).

30. Slobodeniuk, A O, Basko, D. M. Spin–flip processes and radiative decay of dark intravalley excitons in transition metal dichalcogenide monolayers. *2D Mater.* **3,** 35009 (2016).